Climate transition in the Asia inland at 0.8–0.6 Ma related to astronomically forced ice sheet expansion

Article *in* Quaternary Science Reviews · November 2020

DOI: 10.1016/j.quascirev.2020.106580

11 authors, including:

Wenxia Han
Linyi University
39 PUBLICATIONS **479** CITATIONS

Erwin Appel
University of Tuebingen
238 PUBLICATIONS **5,360** CITATIONS

Albert Galy
University of Lorraine
240 PUBLICATIONS **8,810** CITATIONS

Wolfgang Rösler
University of Tuebingen
40 PUBLICATIONS **821** CITATIONS

Quaternary Science Reviews 248 (2020) 106580

Contents lists available at ScienceDirect

Quaternary Science Reviews

journal homepage: www.elsevier.com/locate/quascirev

Climate transition in the Asia inland at 0.8–0.6 Ma related to astronomically forced ice sheet expansion

Wenxia Han [a, b, *], Erwin Appel [b], Albert Galy [c], Wolfgang Rösler [b], Xiaomin Fang [d], Xiuhua Zhu [e], Jef Vandenberghe [f], Jiuyi Wang [g], André Berger [h], Shuang Lü [i], Tao Zhang [d]

[a] Shandong Provincial Key Laboratory of Water and Soil Conservation and Environmental Protection, College of Resources and Environment Sciences, Linyi University, Linyi, 276000, PR China
[b] Department of Geosciences, University of Tübingen, Hölderlinstr. 12, D-72074, Tübingen, Germany
[c] Centre de Recherches Pétrographiques et Géochimiques, UMR7358, CNRS, Université de Lorraine, 54500, Vandoeuvre Les Nancy, France
[d] Key Laboratory of Continental Collision and Plateau Uplift & Institute of Tibetan Plateau Research, Chinese Academy of Sciences, Beijing, 100085, PR China
[e] Center for Earth System Research and Sustainability, CliSAP, University of Hamburg, 20144, Hamburg, Germany
[f] Department of Earth Sciences, VU University Amsterdam, De Boelelaan 1085, 1081, HV Amsterdam, the Netherlands
[g] MNR Key Laboratory of Metallogeny and Mineral Assessment, Institute of Mineral Resources, CAGS, Beijing, 100037, China
[h] Georges Lemaître Center for Earth and Climate Research, Université Catholique de Louvain, Louvain-la-Neuve, Belgium
[i] Qinghai Provincial Key Laboratory of Geology and Environment of Salt Lakes, Qinghai Institute of Salt Lakes, Chinese Academy of Sciences, Xining, 810008, PR China

A R T I C L E I N F O

Article history:
Received 5 June 2020
Received in revised form
1 September 2020
Accepted 5 September 2020
Available online 22 September 2020

Keywords:
Qaidam basin
East asia summer monsoon
Ice sheet expansion
Linear and non-linear time series analysis
Orbital forcing
Westerly jet

A B S T R A C T

Knowing the evolution history of the climate systems in the Asian inland dominated by either the Westerlies or the Asian monsoon, and understanding their associated driving mechanisms are crucial for assessing future trends of climate and environmental conditions in this region, but both the evolution and mechanisms are still under debate. In this study, we present a comparative analysis of massive data from an accurately dated drill core retrieved from the Westerlies controlled western Qaidam Basin (QB), with records from the Chinese Loess Plateau (CLP) dominated by the East Asia summer monsoon (EASM), to track the time and frequency domain evolution patterns and dynamic changes of the QB and the CLP systems. The results infer two main conclusions. First, a critical transition in the evolution of Qaidam paleolake occurred at 0.8–0.6 Ma, characterized by striking changes in proxy variations and a system shift from periodic variations to more irregular fluctuations after 0.6 Ma. Second, a similar evolution pattern prevailed in the Qaidam paleolake region and in the EASM-dominated CLP between ~2.7 and ~1.2 Ma, but a divergence of both systems started at ~1.2 Ma and fully established after 0.6 Ma, when largely fluctuating climate conditions in the QB with a distinct drying trend was accompanied by synchronous largely fluctuated EASM with an increasing trend after 0.6 Ma. We suggest that ice sheet expansion in the Northern Hemisphere, promoted by co-occurrence of low obliquity amplitudes and low eccentricity, drove both systems across a threshold at ~1.2 Ma, and the internal forcing due to glaciation disturbed the previous response of both systems to solar insolation and led to the divergence of two systems. At ~0.9–0.8 Ma, a node of the 1.2-Myr obliquity cycle co-occurred with an eccentricity minimum, which together with coeval decrease in atmospheric CO_2 concentration, could have facilitated a striking expansion of ice sheets. The resulting more equatorial and zonally oriented northern hemisphere westerly jet could serve as key factor leading to the final collapse of Qaidam paleolake after ~0.6 Ma, and the divergence of the QB and the CLP systems.

1. Introduction

The climatic systems dominated by the Asian monsoon and the Westerlies bear crucial signals to understand the interaction between sub-systems (e.g., high latitude ice sheets, marine

* Corresponding author. Shandong Provincial Key Laboratory of Water and Soil Conservation and Environmental Protection, College of Resources and Environment Sciences, Linyi University, Linyi, 276000, PR China.
E-mail address: wenxia_han@163.com (W. Han).

https://doi.org/10.1016/j.quascirev.2020.106580
0277-3791/

environments, and mid-latitude inland areas) and thus affecting future evolution of Earth' climate, because the Asian monsoon system straddles over two hemispheres, and the Westerlies occupy much of the mid- and high-latitudes of the northern hemisphere. Modern-day western Asia is dominated by arid and semi-arid conditions, and its climate is considered to be controlled by the Westerlies, while the climate of the adjacent Chinese Loess Plateau (CLP) is under the influence of the East Asian summer monsoon (EASM) and relatively more humid (Chen et al., 2008, 2019; An et al., 2012; Curio et al., 2015; Wang et al., 2017). Understanding the temporal evolution of these two systems during the Quaternary provides a basis to reveal the evolution pattern of different systems in the Asia inland and to unravel the possible effects of external (e.g., solar insolation) and internal (e.g., ice sheets evolution, tectonic activity) forcing on the Asia climate, which is significant for predicting future climate and ecological conditions in the Asia inland under global warming and increasing melting of the two hemisphere ice sheets. However, the evolution patterns of the Westerlies and monsoon-dominated regions in Asia are still under debate, with some studies arguing for a consistent evolution pattern on orbital and sub-orbital scales (e.g., Ding et al., 2002; Yang et al., 2006; Li et al., 2016) and others proposing an out-of-phase relationship (Chen et al., 2008, 2019) between the two systems. The discrepancy in the interpreted evolution pattern of different systems in Asia led to controversial views on related driving mechanisms, including interplays of external solar insolation and global ice volume (e.g., Liu and Ding, 1993; Ding et al., 1995), global cooling (e.g., Lu et al., 2010; Yang et al., 2013a; Koutsodendris et al., 2018), or combined global cooling and tectonic activity (e.g., An et al., 1990; Fang et al., 1999; Xiao and An, 1999; Han et al., 2014a).

Aiming to solve the described controversies, we studied an accurately dated deep drilling core (SG-1; 938.5 m in depth, spanning 2.7–0.08 Ma, Zhang et al., 2012a) retrieved from the western Qaidam Basin (QB), where the water vapor is primarily supplied by the Westerlies (Xu et al., 2008; Curio et al., 2015), and out of the northern and western reach of the modern Asian summer monsoon (Gao, 1962) (Fig. 1). We compare its (published and newly obtained) records with records from the CLP where the EASM system dominated. The previous studies of the SG-1 core indicate the existence of a semi-deep lake in the western QB in the early Quaternary, and a long-term stepwise drying that finally terminated in a salt playa (e.g., Wang et al., 2012, Zhang et al., 2012b; Yang et al., 2013a, b, 2016; Herb et al., 2015a; Koutsodendris et al., 2018). These results provide fundamental information on the evolution history in the Westerlies dominated QB, which in terms of drying is roughly consistent with the evolution observed in records of the monsoon dominated CLP (An et al., 1990; Liu and Ding, 1993; Song et al., 2001; Sun et al., 2010). Further investigation of the detailed evolution pattern of records from these two systems bear great potential to recognize whether moisture conditions in these two systems evolved equally or differently in specific periods of the Quaternary. Such kind of comparative studies are still missing, or merely based on visual comparison between different records. More advanced information, such as identification of critical transitions in both systems and their potential driving forces that are vital for the future prediction of their evolution pattern, calls for more comprehensive studies than preliminary visual comparisons.

We thus performed statistical analyses and linear time series analyses on proxy records to capture the detailed evolution pattern in time and frequency domain, and nonlinear recurrence analyses, which has been successfully applied to determine dynamical changes and transitions in paleoclimate studies that cannot be revealed by visual examination or linear methods (Marwan et al., 2007, 2017; Donges et al., 2011; Eroglu et al., 2016). These comprehensive analyses can, on the one hand, reveal more robustly the detailed evolution history of the studied QB and CLP systems and the occurrence of critical transitions. They can also help to track the history of the response of QB and CLP systems to external or internal driving forces, retrieved from the nonlinear recurrence quantification analysis. Therefore, we organize this paper as presenting the evolution history of the Qaidam paleolake and identify a critical transition in its evolution from a semi-deep lake to salt playa in section 3.2. We then compare these results from the Westerlies controlled western QB with published results from the monsoon dominated CLP in part 3.3. In section 3.4, we discuss the possible associated driving forces on the Quaternary evolution of the two systems.

2. Materials and methods

2.1. Proxy records from the SG-1 core

We perform a comprehensive analysis on groups of proxies and on single high-resolution proxy records to obtain more robust information than provided by previous results that are mostly based on single parameters. We use proxies from core SG-1 (published and new), which are available at high resolution and can provide complementary information. They comprise records of published acetic acid-leached manganese content (Mn_{HOAc}) (N = 870) from Yang et al. (2013a, 2017), mass-specific magnetic susceptibility (χ) (N = 2985) from Zhang et al. (2012b), carbonate $\delta^{18}O$ and $\delta^{13}C$ data from the depth interval of 0–600 m from Han et al. (2014a), supplemented by new $\delta^{18}O$ and $\delta^{13}C$ measurements mainly from marl layers with high carbonate content (>30 wt%) throughout the entire core (total N = 538), and new mean grain-size (Mz) (N = 4288) data. Other proxy records, such as magnetic properties (Zhang et al., 2012b; Herb et al., 2013, 2015a) and lower resolution elements records obtained after acetic acid leaching by Yang et al. (2014, 2016), are additionally used for multivariate statistical analysis.

The new isotope data were measured on a MAT-252 (Delta-E) gas source isotope mass spectrometer and the results are expressed using the δ notation relative to the PDB standard (with precision better than 0.1‰ for both $\delta^{18}O$ and $\delta^{13}C$). Grain-size distributions were measured using a Microtrac S3500 laser particle sizer at the Institute of Tibetan Plateau Research, Chinese Academy of Sciences following the procedure of Lu and An (1997). GRADISTAT Version 6.0 was used to generate grain-size statistics (Blott and Pye, 2001).

2.2. Statistical and time series analysis

In our analyses, we aim to detect structures of the proxy records along the geological time axis, qualitatively and quantitatively, which then are used as the basis for interpreting features and transitions in the climate and paleolake evolution. Our approach to identify structural features includes standard methods such as multivariate statistics and linear time series analysis, but also nonlinear time series analysis to check for irregularities in the periodical behavior. For dating, we use the SARA age model established for core SG-1 by Herb et al. (2015b), based on orbital tuning of magnetic susceptibility, with anchor points from magnetostratigraphy (Zhang et al., 2012a) and from OSL and U-series dating (Han et al., 2014b).

We start our analytical approach with extracting climate-related features of multivariate parameter combinations versus geological age. For this purpose, we chose Fuzzy C-Means (FCM) cluster analysis, which is frequently and widely used for pattern recognition. FCM results provide membership functions, which

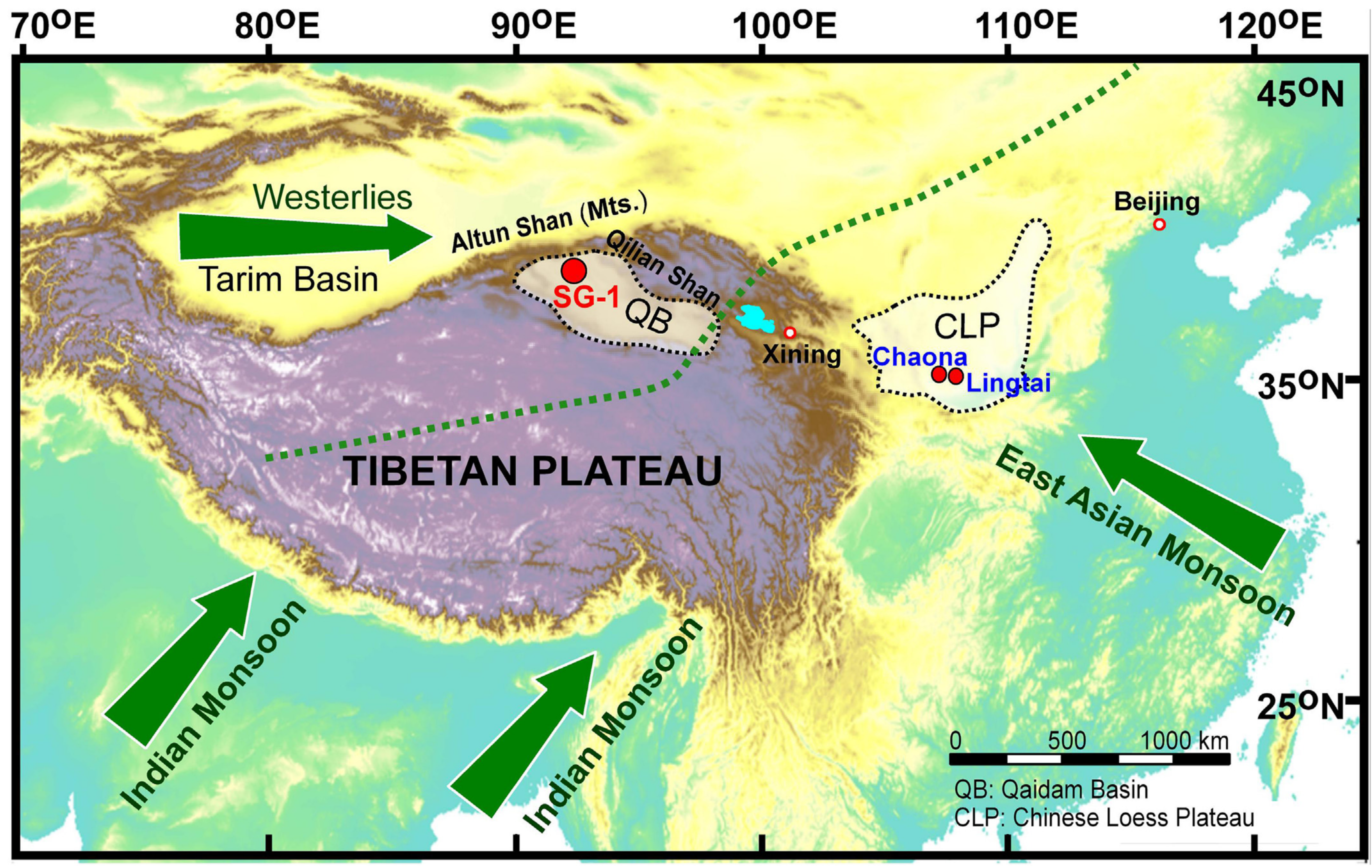

Fig. 1. Map of the study region and the principle trajectories of atmospheric circulation. Locations of the drill core SG-1 in the Qaidam Basin, and of the Lingtai and Chaona loess sections from the Chinese Loess Plateau are displayed. The green dashed line shows the present reach of the Asian summer monsoons (Gao, 1962). (For interpretation of the references to color in this figure legend, the reader is referred to the Web version of this article.)

quantitatively show the likelihood that a sample is associated with pre-defined clusters. Combinations of proxy parameters for FCM cluster analysis were selected by two criteria. First, the parameters should be sufficiently complementary (i.e. not duplicating information), and second, their paleoclimate meaning should be understood reasonably well. Dissimilarity was tested by linkage distances in a dendrogram analysis after common data standardization. For dendrogram analysis we included 23 proxy data sets (published and new data) of the SG-1 core: rare earth elements (Yang et al., 2014), magnetic properties (Zhang et al., 2012b; Herb et al., 2013, 2015a), carbonate content (Han et al., 2014a), acid soluble elements (Yang et al., 2013a, 2016, 2017), mean grain-size (new data) and stable isotope data (Han et al., 2014a; and new data). Several suitable parameter combinations were then processed by FCM cluster analysis. Both dendrogram analysis and FCM cluster analysis were performed with the Matlab software. To obtain information on regular periodicities in the variability of the proxy parameters versus geological age, we applied conventional linear time series analysis by calculating wavelet power spectra (WPS). The WPS analysis was performed using the Matlab package with the script of Torrence and Compo (1998).

We further analyzed the evolutionary variability in individual proxy data sets versus mean values. Means were calculated along the records using a rectangular sliding window, and within the sliding windows variances of the original data were determined after detrending with the mean values. To obtain information about variabilities beyond orbital variations, we chose a 200-kyr window length that is the shortest possible window eliminating efficiently orbital variations. However, 400-kyr, 100-kyr, 41-kyr and 21-kyr windows were also tested (see Supplementary Fig. S1 and Text S1 for details) to ensure the robustness of the results.

Moreover, using the individual proxy time series data, we determined so-called recurrence plots and performed recurrence quantification analysis. Detailed information about them can be found in Marwan et al. (2007, 2017) and Eroglu et al. (2016). Below, we restrict on a short overview of possibilities and meanings of this approach; in the Supplementary Text S2 we summarize more details. Recurrence analysis is a nonlinear approach which can detect dynamical features in the phase-space transform of time series data, which are hidden in the results of conventional time series analysis results such as bandpass-filtering, WPS, or Fourier transforms. It could reveal instabilities of periodic behavior, i.e., provide a quantification of how periodic or chaotic or even stochastic the observed variability in a parameter record is. Recurrence quantification results allow to test the possible occurrence of changes in the system behavior, which may represent tipping points of the system.

Recurrence plot is a binary plot, in which stochastic or chaotic climate fluctuations (i.e., less predictable, unstable) lead to isolated recurrence points or short lines of points in the plot, whereas periodic processes (i.e., highly predictable, more stable) produce longer diagonal lines (Marwan et al., 2007). The point distribution can be quantified by various parameters. In this study, we use the determinism, which calculates the fraction of points in the recurrence plot that form diagonal lines with respect to all points (Marwan et al., 2007). Higher determinism indicates more periodic behavior, and extreme changes of determinism values identify times with prominent shifts between different regimes (e.g., Marwan et al., 2007, 2017), which are crucial to identify critical transitions in the studied system and to explore possible variations in the driving mechanism(s). The original unevenly spaced data of the SG-1 core was transformed using the new Transformation Cost Time Series method, whose principle is to calculate the shortest distance (lowest transformation cost) of transforming one segment of the record into the following segment (Eroglu et al., 2016), to evenly spaced data. We use 6.9, 9.1, 12.1 and 2.7 kyr, as the segment sizes of the χ, Mn_{HOAc}, $\delta^{18}O$ and Mz records, respectively, to transform these four original data to evenly spaced records for further recurrence analysis. The recurrence analysis was performed using the Cross Recurrence Plot toolbox of Marwan et al. (2007), with an adaptively chosen threshold distance that ensures a constant recurrence rate of 10%.

3. Results and discussion

3.1. Proxy results of the SG-1 core and their environmental implications

The profiles of $\delta^{13}C$ and $\delta^{18}O$ (published and newly obtained data) show a long-term persistent increase in $\delta^{18}O$ along the entire core and evident increases to heavier isotope compositions above 1.2 Ma and 0.6 Ma (Fig. 3E). The $\delta^{18}O$ ($\delta^{13}C$) values (Fig. 2 and Fig. 3E) remain at low mean levels of −0.23‰ (1.23‰) from 2.7 to 1.9 Ma, and to −0.68‰ (0.97‰) from 1.9 to 1.2 Ma. The values then increase significantly to mean values of −0.63‰ (1.21‰) from 1.2 to 0.6 Ma, and of 1.97‰ (2.32‰) from 0.6 Ma upwards. The scatter plot of $\delta^{13}C$ versus $\delta^{18}O$ (Fig. 2) shows an approximate linear relationship, indicating that the carbonate fraction of the marls was precipitated predominantly within a closed basin (Stuiver, 1970; Talbot, 1990). The large difference in $\delta^{13}C$ and $\delta^{18}O$ values in the sediments of core SG-1 compared with the carbonate rocks of the surrounding mountains (Fig. 2) confirms that the carbonates in sediments were mostly precipitated *in situ* within the lake, therefore, they represent the environmental conditions at the time of deposition (Han et al., 2014a). Evaporation is thus considered to be the major control on variations in the carbon and oxygen isotope composition of sediments in the SG-1 core (Han et al., 2014a). So, we interpret the long-term increase in $\delta^{13}C$ and $\delta^{18}O$ values as representing a gradual drying of the paleolake since 2.7 Ma and accelerated shrinkage/drying at about 1.2 Ma and 0.6 Ma. Comparison of the $\delta^{13}C$ and $\delta^{18}O$ values of SG-1 core with those of modern lakes from elsewhere in the world (McKenzie, 1985; Talbot, 1990; Talbot and Kelts, 1990) indicates that the period from 2.7 to 1.2 Ma falls mainly within the range of a brackish lake, while those after 0.6 Ma reflect a salt lake, and the values during 1.2−0.6 Ma represent an intermediate stage (Fig. 2).

This result is consistent with the evolution of Mn_{HOAc} in core SG-1 (Fig. 3D) which indicates a long-term decrease in the input of Mn derived from catchment weathering and the increasing oxidation of the lake bottom water since 2.7 Ma (Yang et al., 2013a). The Mn_{HOAc} is interpreted as a sensitive indicator of the evolution of lake redox conditions and catchment-scale climate change (Yang et al., 2013a). During warmer and wetter intervals, the increased input of Mn from the rocks and soils in the drainage area and the transformation of Mn oxides under conditions of higher lake level and oxygen-deficient bottom water lead to higher values of Mn_{HOAc}.

Detailed rock magnetic analyses (Zhang et al., 2012b) and the comparison of the magnetic susceptibility (χ) record with the *Artemisia*/*Chenopodiaceae* (A/C) pollen ratio for the interval of ~1.25−0.75 Ma indicate that χ is a sensitive proxy for moisture changes in the catchment of the Qaidam paleolake, with higher and lower values representing drier and wetter conditions, respectively (Herb et al., 2015a). However, the correlation of the χ and the A/C

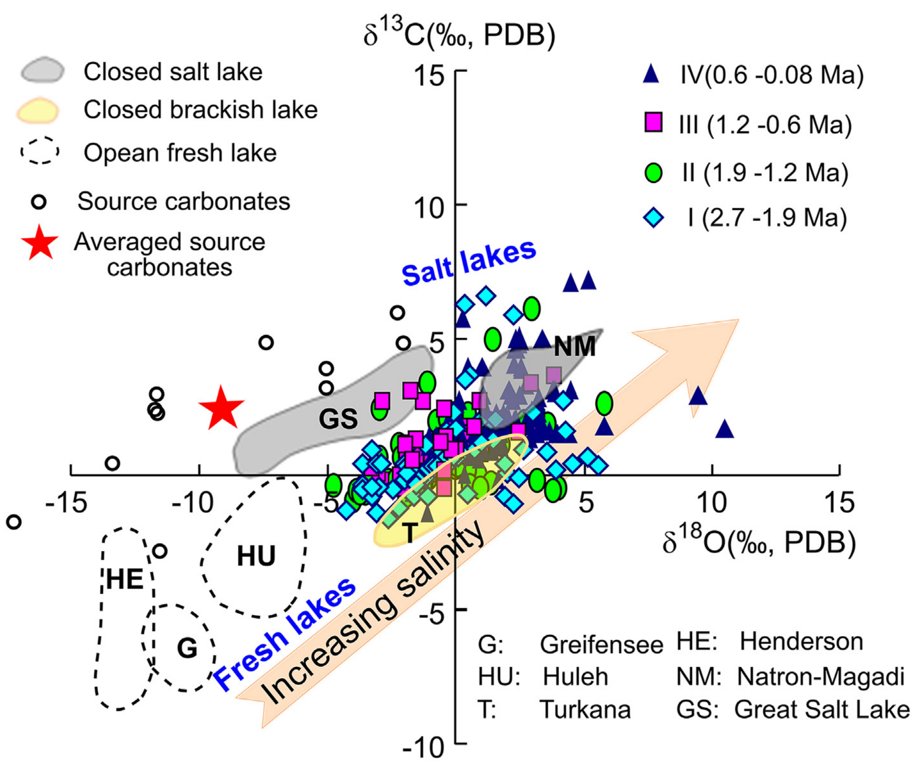

Fig. 2. Scatter plot of carbon and oxygen isotope values from carbonates in different phases of the SG-1 sequence, compared to the values of modern globally-distributed open and closed lakes with different salinities (McKenzie, 1985; Talbot, 1990; Talbot and Kelts, 1990), revised from Han et al. (2014a).

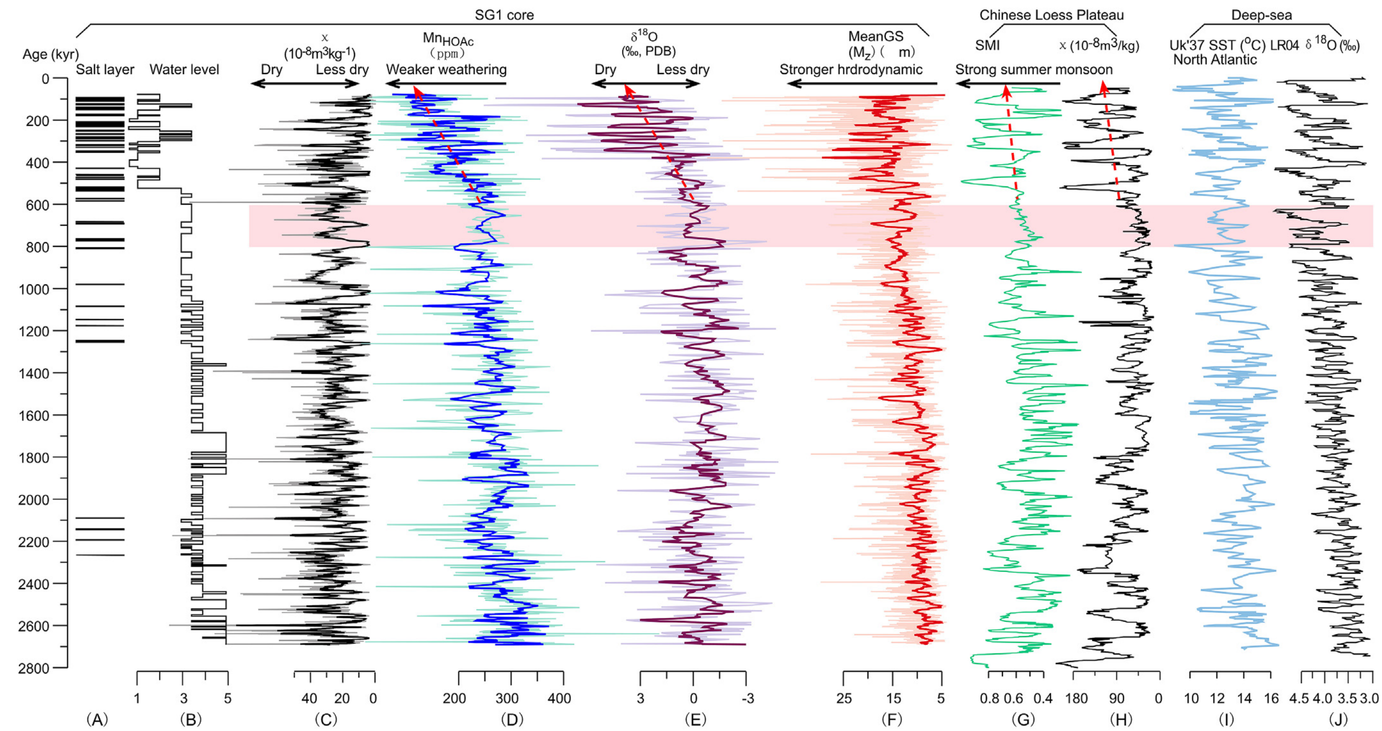

Fig. 3. (A–F) Proxy records from drill core SG-1: (A) Salt layers occurrence and (B) water level (Wang et al., 2012), (C) magnetic susceptibility (χ) (Zhang et al., 2012b), (D) acetic acid-leached manganese content (Mn_{HOAc}) (Yang et al., 2013a, 2017), (E) $\delta^{18}O$ (Han et al., 2014a; and new data), (F) mean grain-size (Mz) (new data); thick lines represent 5-point smoothing of χ, Mn_{HOAc} and $\delta^{18}O$, and 15-point smoothing of Mz. Climate implications of the four records are briefly mentioned on the top; for further explanation see text. (G–J) Comparison with other regional and global climatic records: (G) Summer monsoon index (SMI) (Sun et al., 2010) and (H) magnetic susceptibility (χ) record (Song et al., 2001) both from the Chinese Loess Plateau; (I) alkenone sea-surface temperature (SST) record from the North Atlantic Ocean (Lawrence et al., 2009), (J) LR04 stacked marine $\delta^{18}O$ record (Lisiecki and Raymo, 2005). The pink shaded bar displays the interval between ~0.8 and 0.6 Ma characterized by very low fluctuations in proxy records of the SG-1 core and the EASM system. (For interpretation of the references to color in this figure legend, the reader is referred to the Web version of this article.)

ratio is disturbed in parts of the SG-1 sequence, interpreted by the additional influence of catchment changes (Herb et al., 2015a), which is most evident for the decreasing values after ~0.5 Ma. The χ record is therefore a mixed signal.

In the lake catchment sedimentary system, debris, transported by rivers or by wind enters the lake, are re-dispersed, mixed and deposited under the influence of hydrodynamic processes. The mean grain-size (Mz) is therefore a measure of the grain-size distribution of sediments delivered to the lake by fluvial and eolian processes and reflects the energy of the hydrodynamic and eolian processes during transport and deposition. We interpret the increase in Mz from the bottom to the top of core SG-1 as an increase in the strength of wind energy and hydrodynamic processes. The basal part of the core is very fine-grained, apparently due to large content of the 2–5 μm sediments (Wang, 2012). This fraction represents settling of suspended material in lacustrine environment, probably from direct air fall (Vandenberghe et al., 2018). In contrast, the upper part of the record is much coarser (coarse silts; Wang, 2012) and may represent either windblown material supplied from saltation or fluvial reworking (Vandenberghe, 2013). This confirms the transition towards drying of the lake as observed by the other proxies.

Lake-level reconstruction based on lithology also supports the progressing drying (Wang et al., 2012) (Fig. 3B), showing that a semi-deep fresh water to semi-brackish lake during ~2.7–2.5 Ma was replaced by a perennial saline lake after ~1.2 Ma, and eventually by saline mudflats and a playa salt lake after ~0.6 Ma. Moreover, the long-term drying of the western QB since the late Paleocene is supported by pollen records from SG-1 core (Koutsodendris et al., 2018) and another long drill core from the western QB (Cai et al., 2012), and from synthesis results of several other cores from the QB (Kang et al., 2003). Loess records from the Tarim Basin (Fang et al., 2002; Zan et al., 2010) reveal a synchronous expansion of the Mu Us Desert (Ding et al., 2005) and the Gurbantunggut Desert in northwest China (Fang et al., 2002), also suggesting a major aridification trend within a large region of Central Asia at this time.

3.2. Evolution and critical transitions of the Qaidam paleolake

In this section we use the results of the linear and nonlinear analyses to reveal the evolution pattern of the Qaidam lake system since 2.7 Ma, summarizing key features and identifying critical transitions. We start the discussion with the overview of stages in the evolution identified by the FCM cluster results, then we present the variance-vs-mean results, which also show the evolution of stages, but add information on trends and variabilities beyond orbital variations. The presence and evolution of orbital periodicities as shown by the WPS results follows as a linear feature in the analyzed time series. Finally, the results of recurrence analysis are presented and discussed with the aim of recognizing system changes from nonlinear dynamic features in the proxy time series.

3.2.1. Statistical analysis

The FCM cluster analysis based on different data proxy combinations reveal a similar pattern of clusters for the SG-1 sequence. A three-cluster solution provides the best discrimination between clusters and the clearest pattern of evolution. The results shown in Fig. 4A are displayed as a typical example (there are many other combinations with essentially the same features of the cluster evolution). The input data for this combination comprises three

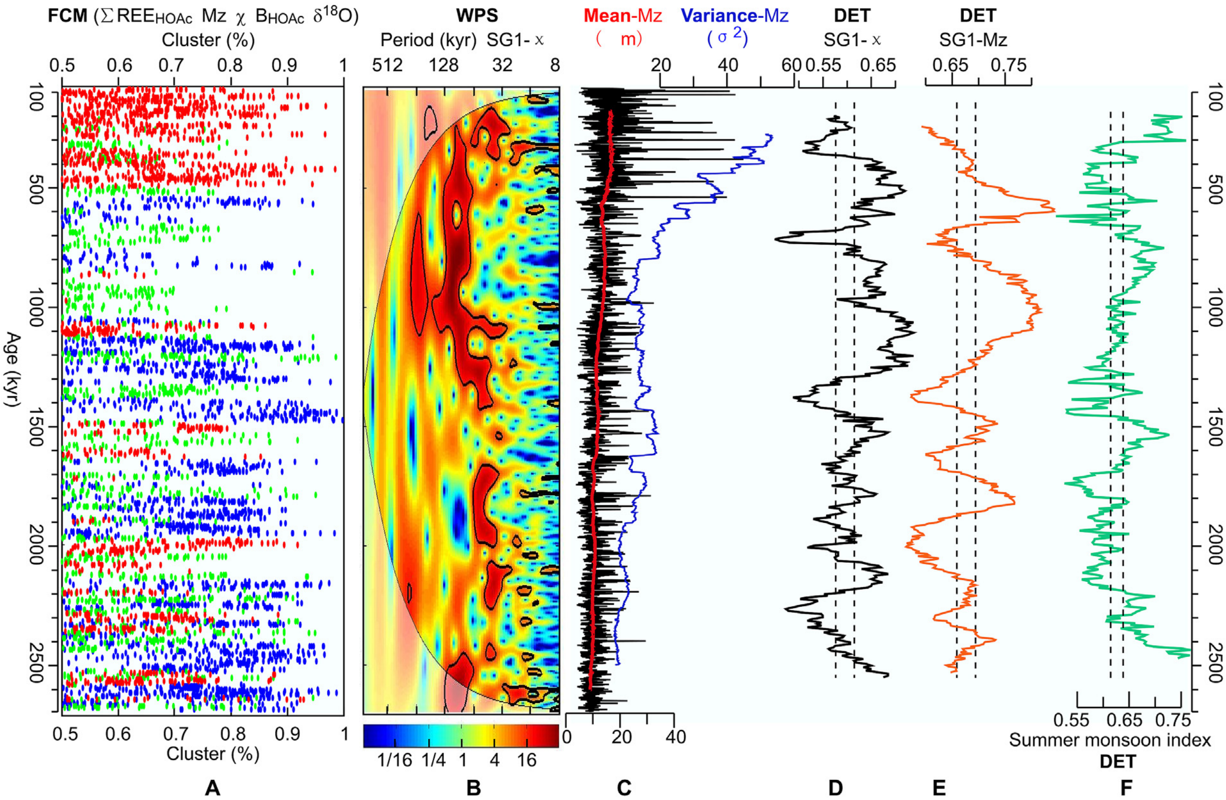

Fig. 4. Comprehensive results based on proxy time series of the SG-1 core. (A) Membership probability of fuzzy C-means cluster analysis (FCM) results for Mz − χ − $\delta^{18}O$ − boron concentration (B_{HOAc}) − total abundance of rare earth elements ($\sum REE_{HOAc}$) data from the SG-1 core (3-cluster solution). C1 (red) represents dry conditions, C2 (blue) represents less dry condition, and C3 (green) represents intermediate conditions (see text for details). (B) Results of wavelet power spectrum analysis of the SG-1 χ record, (C) Sliding window means (red) of the SG-1 Mz record (black) and variances (blue) of the detrended original curve (200-kyr sliding window); (D–F) System determinism (DET) calculated from SG-1 χ and Mz and summer monsoon index from the Chinese Loess Plateau (Song et al., 2001) (95% confidence bounds are displayed by dashed lines; they are derived by 1σ-ranges of DETs obtained from 1000-times random re-sampling of the time series values). (For interpretation of the references to color in this figure legend, the reader is referred to the Web version of this article.)

data sets displayed in Fig. 3 (Mz, χ, $\delta^{18}O$), and additional published data sets of boron concentration (B_{HOAc}) and the total abundance of rare earth elements ($\sum REE_{HOAc}$), both obtained after acetic acid leaching (Yang et al., 2014, 2016). $\sum REE_{HOAc}$ is a sensitive proxy for the intensity of chemical weathering and climatic conditions within the drainage area (Yang et al., 2014), and B_{HOAc} can be interpreted as an indicator of lake water salinity (Yang et al., 2016).

Cluster one (C1, red) is characterized by higher $\delta^{18}O$, B_{HOAc} and Mz, and lower $\sum REE_{HOAc}$, suggesting a drier climate and weaker chemical weathering. In cluster two (C2, blue), $\sum REE_{HOAc}$ is high and $\delta^{18}O$, B_{HOAc}, χ and Mz are relatively low, which is interpreted as relatively less dry climate and stronger chemical weathering. Cluster three (C3, green), with all of the values between those of C1 and C2, indicates an intermediate state. The cluster pattern in Fig. 4A reveals five stages of the lake system evolution. *Stage I (~2.7-1.1 Ma)* is characterized by a less dry climate (cluster C2) with the occurrence of a drier phase (cluster C1) every ~400 kyr, at around 2.4–2.3 Ma, 2.1–2.0 Ma, 1.6–1.5 Ma, and 1.1 Ma. *Stage II (~1.1-0.8 Ma)* is characterized by decreased cluster variability at intermediate conditions (cluster C3). *Stage III (~0.8-0.5 Ma)* reveals the return of less dry conditions (cluster C2*). Stage IV (since ~0.5 Ma)* is characterized by clear dominance of dry climate (cluster C1). In *Stage V (since ~0.3 Ma)* only the dry cluster (cluster C1) occurs.

Time-dependent sliding window means of the SG-1 $\delta^{18}O$, Mn_{HOAc}, χ and Mz records, and variances (σ^2) of the detrended original curves (Fig. 5) reveal some remarkable features in the environmental evolution of the QB. We present the results obtained for 200-kyr (Fig. 5) as this window length allows the best possible time resolution at simultaneously averaging out orbital variations (see Supplementary Text S1 and Fig. S1). The results show the following features: (1) A long-term increase/decrease of the mean values in $\delta^{18}O$, Mz and χ records/in Mn_{HOAc}, reflecting a long-term increase in lake evaporation, the strength of wind energy and hydrodynamic processes, and decreased moisture in the catchment of the Qaidam paleolake (Herb et al., 2015a); (2) a striking increase in the variance in $\delta^{18}O$ and Mz, and an increasing trend in the variance of Mn_{HOAc} and χ records since ~0.6–0.5 Ma; (3) the correlation between mean and variance of the records from core SG-1 shows no or low correlation between 2.6 and 0.5 Ma, but high correlation after ~0.5 Ma (Fig. 5 and Supplementary Fig. S2). These characteristics, together with the striking increase in the variance of the proxy records, indicate an important climate transition at ~0.6–0.5 Ma.

3.2.2. Wavelet analysis

The wavelet analysis results of χ (Fig. 4B), Mz, Mn_{HOAc} and $\delta^{18}O$ (Supplementary Fig. S3G-J) reveal pronounced cyclicities of 100-kyr, 54-kyr and 41-kyr throughout the core, and there is a generally very low spectral power during ~0.8–0.6 Ma in the wavelet results of Mn_{HOAc} and $\delta^{18}O$. The dominance of 41- and 54-kyr cycles (likely obliquity) in the lower part of the core, the appearance ($\delta^{18}O$, χ) or strengthening (Mz) of periodicities near 100-kyr (likely eccentricity) starting at ~1.4–1.2 Ma, and the re-dominance of the obliquity cycles after ~0.4–0.3 Ma, are important common features

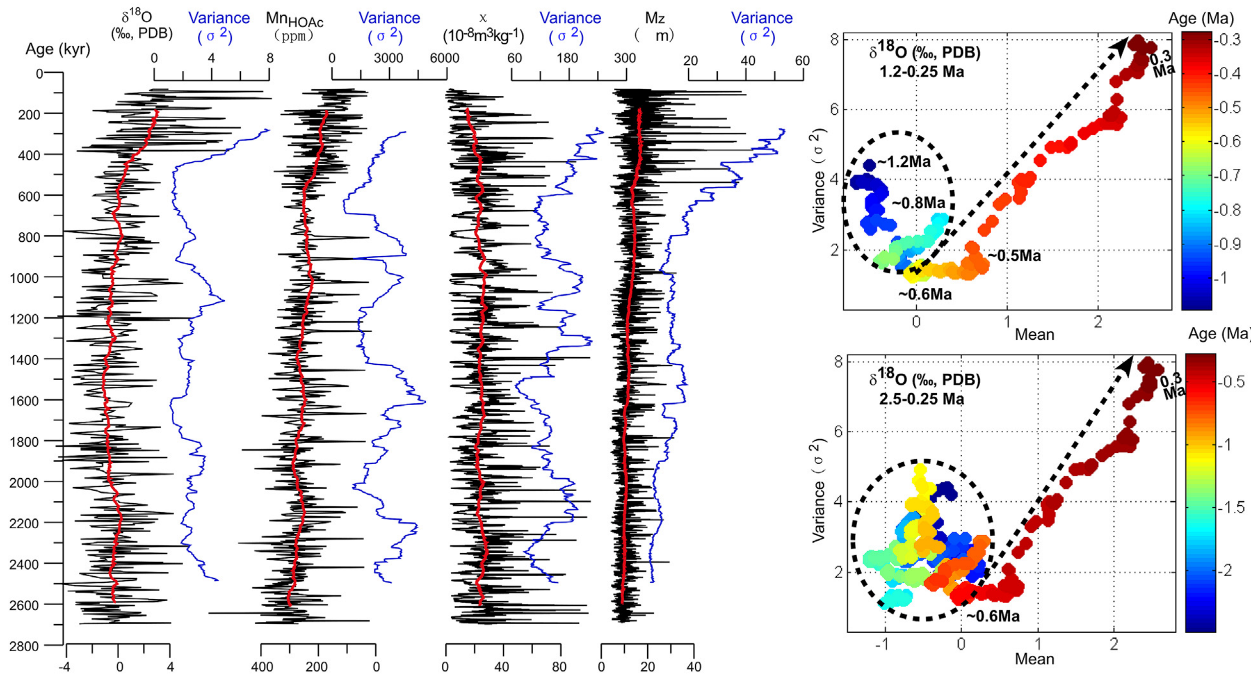

Fig. 5. (Left) Sliding window means (red) of the $\delta^{18}O$, Mn_{HOAc}, χ and Mz records (black) from core SG-1 (200-kyr sliding window) and variances of the original time series values within the sliding windows after detrending with the sliding window means. (Right) Scatter plots of variance versus mean; the color code shows the time of window centers from 2.6 Ma to 0.25 Ma, and 1.2 Ma to 0.25 Ma. No or low correlation between mean and variance appears before ~0.5 Ma, but high correlation occurs afterwards. (For interpretation of the references to color in this figure legend, the reader is referred to the Web version of this article.)

in the wavelet records. There is also an indication of the 21-kyr precession cycle in parts of the core, but the remaining uncertainties in the age model and the different resolution of proxies records, preclude the further discussion of the precession cycle. Periodicities near the 400-kyr eccentricity cycle are also visible throughout the Mz record (Supplementary Fig. S3H) and in χ and Mn_{HOAc} (Supplementary Fig. S3G, I) between ~2.6 and ~1.2 Ma. Prominent periodicities near 200 kyr after ~1.3 Ma in Mz and χ records were interpreted as a resonance effect of the 100-kyr cycle (Herb et al., 2015b).

3.2.3. Recurrence plots and recurrence quantification analysis

Non-linear structures of proxy time series can help to reveal regime/system changes than one cannot see by visual examination or linear methods. We generate recurrence plots and performed recurrence quantification analysis on SG-1 χ, Mn_{HOAc}, $\delta^{18}O$ and Mz records to identify changes in the evolution of the Qaidam paleolake. The recurrence plots show a prominent transition from previous long diagonal or vertical/horizontal lines to single points/very short lines after ~0.6 Ma (Fig. 6A–D). The determinism results of the proxy records from core SG-1 display four intervals with high determinism, at about 2.6–2.4 Ma, 2.1–1.6 Ma, 1.2–0.8 Ma, and 0.6–0.4 Ma, and a shift from high to low determinism values at ~2.4 to ~2.2 Ma, ~1.45 to ~1.2 Ma, ~0.8 to ~0.6 Ma and after ~0.4 Ma (with slight differences between proxies) (Fig. 4D–E and Supplementary Fig. S3C-F), indicating substantial changes in lake dynamics during these four transition intervals.

3.2.4. Critical transitions in the Qaidam paleolake evolution

In this section we summarize key features in the evolution of the

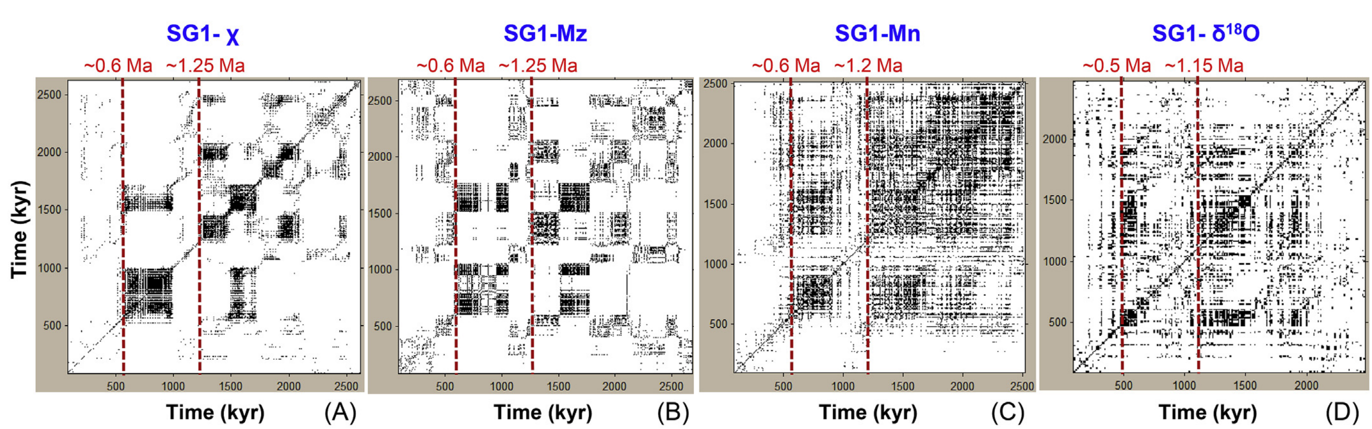

Fig. 6. Recurrence plots for records of χ (A), Mz (B), Mn_{HOAc} (C) and $\delta^{18}O$ (D) for core SG-1. A transition in recurrence plots from longer diagonal or vertical/horizontal lines before ~0.6 Ma to single points or very short lines afterwards indicate a prominent system change from higher predictability to more erratic environment (Marwan et al., 2007).

Table 1
Summarized key features in the evolution of the Qaidam lake system indicated by the results of methods applied on the SG-1 proxies.

Stage Age (Ma)	FCM cluster analysis	Wavelet analysis	Mean versus variance	Recurrence quantification
Stage V **~0.3–0.08**	Very dry climate (C1 cluster only)	Reappearance of 41-kyr cyclicity	Pronounced change in the mean and trend to high variance;	Shift to low determinism
Stage IV **~0.6–0.3**	Dominance of dry climate (C1 cluster dominant)	~100-kyr cyclicity dominant in all records	High correlation between mean and variance	Stable high determinism
Stage III **~0.8–0.6**	Return of less dry conditions (C2 cluster reappears)	Low spectral power in Mn_{HOAc} and $\delta^{18}O$ records	Fading of variability in the variance of the proxies	Drop in determinism with the lowest value in the χ record
Stage II **~1.2–0.8**	Decreased cluster variability with intermediate conditions (more important C3 cluster)	Transition to dominant ~100-kyr cyclicity	Long-term trend of the mean values of all four proxies; no or low correlation between mean & variance	Return to stable high determinism
Stage I **~2.7–1.2**	Dominated by a less dry climate (C2 cluster) with dry events every ~400 kyr	Main periodicities near 100-kyr and 54–41-kyr		High determinism and two pronounced lows at 2.3–2.2 and ~1.4 Ma

Qaidam lake system, based on the results and discussion of the previous section (Table 1). It is clear that the four proxy records (SG-1 χ, Mn_{HOAc}, $\delta^{18}O$ and Mz) do not display exactly the same features, with lower amplitude, and/or with slight time difference due to different resolution or controlling factors on different proxies. We roughly separate the lake evolution into five main stages based on these features (Fig. 4): *Stage I (~2.7 to ~1.2 Ma)* is dominated by less dry climate with intercalated dry events at every ~400 kyr. Main cyclicities near 100-, 54- to 41-kyr in the wavelet records corroborate a periodic evolution at this stage. There are two marked lows in the determinism records (especially in the χ record) during ~2.3–2.2 Ma and at ~1.4 Ma. Sharp determinism drop following an extended higher determinism indicate a transition from a more predictable (e.g., periodic) system to an unstable (less predictable) one (Marwan et al., 2007, 2017). The shift of system behavior and the establishment of unstable systems during ~2.3–2.2 Ma and at ~1.4 Ma represent critical events in the evolution, but they did not drive the lake system to a critical condition (critical threshold) since the lake recovered again. *Stage II (~1.2 to ~0.8 Ma)* is characterized by increased aridity, a transition to a dominant cyclicity near 100-kyr, and a decrease in the FCM cluster variability during the second half of that stage. A pronounced minimum in determinism at ~1.4 Ma in the proxy records is succeeded by stable high determinism values between ~1.2 Ma and ~0.8 Ma. The *Stage III (~0.8 to ~0.6 Ma)* bears no clear drying trend and the FCM cluster results even indicate somewhat less dry conditions in the second half of that stage. The most notable features are the fading of variability in the variance records of the proxies, and the drop of determinism, especially in the SG-1 χ record. A decrease of determinism in χ record started at 0.76 Ma and rapidly reached the lowest value at 0.72 Ma (Fig. 4D). This sharp shift from stable to extremely unstable lake system could have profound effects to the Qaidam paleolake. The subsequent changes in *Stage IV (~0.6 to ~0.3 Ma)*, which is characterized by strong increase in aridity shown by the stable dry cluster in the FCM, and large variances, indicate a different condition in lake system than before. The correlations of the means and variances of the four analyzed proxy records is another striking feature of the data (Fig. 5). It may be explained by the establishment of a predominantly dry climatic phase, with pulses of drier conditions. During *stage V (after ~0.3 Ma)* an even drier condition dominates the climate system, indicated by FCM cluster result, a reappearance of 41-kyr cyclicity in wavelet results, and marked decrease in determinism (~0.3 Ma) happened in all four records (Supplementary Fig. S3C-F), indicating another regime change event in lake system.

Previous studies have identified several statistical features related to the occurrence of a bifurcation including increasing autocorrelation, increasing return time from perturbations, and increasing variance and skewness related to the occurrence of a 'critical slowing down' (Wissel, 1984; Scheffer et al., 2009; Lenton, 2011). The determinism of the records from the SG-1 core exhibit a striking minimum at ~0.7–0.6 Ma following a proceeding high level (Fig. 4D, E, S3C–F), and a transition in recurrence plots from longer diagonal or vertical/horizontal lines before ~0.6 Ma to single points or very short lines afterwards (Fig. 6A–D). These features indicate a prominent regime change from relatively periodic (higher predictability) to more chaotic or stochastic behavior (less or not predictable) (Eckmann et al., 1987; Marwan et al., 2007, 2017; Eroglu et al., 2016). In the FCM cluster results, a very low cluster variability with dominating of less dry cluster conditions shifts abruptly to a stable arid cluster at this time. In all four records, at ~0.6 Ma there is a transition from a stable state with low variability to a highly fluctuating state with substantial changes in mean values, representing a shift towards increasingly arid conditions with high variability (Fig. 3C–F and Fig. 5), and a sharp drop of the lake level (Fig. 3B). In addition, the high correlations between the moving average of the means and variances after ~0.6 Ma (Fig. 5) indicate pulses of fluctuating conditions and an unstable mean. These features collectively suggest that at ~0.6 Ma the Qaidam lake system approached a critical condition that may represent a possible tipping point. At this time the relatively stable lake system collapsed with a drying trend from which there was no recovery, ending with the formation of a saline mudflat and playa environment (Wang et al., 2012).

This critical transition from stable and predictable system dynamics to a more chaotic/stochastic system which occurred in the western QB during 0.8–0.6 Ma is consistent with records from other areas. Based on data from twelve sediment cores from the subtropical South Atlantic, Schmieder et al. (2000) considered that the interval during 0.92–0.64 Ma represents a third state of global ocean circulation in addition to those before and afterwards. The probability density function of the oxygen isotope record of ODP Site 677 (Shackleton et al., 1990) indicates bifurcation behavior at ~0.725 Ma (Mudelsee and Stattegger, 1997). Huybers (2009) suggested that Pleistocene glacial variability is chaotic and that the transition from the 41 kyr–100 kyr modes of variability at around 0.9 Ma could have occurred spontaneously. This conclusion is supported by studies in which a transition from a primarily linear climate system to a complex, nonlinear system characterized by rapid changes in mean, standard deviation, periodicities, and bifurcation behavior, was suggested to have occurred at this time (Maasch and Saltzman, 1990; Ghil, 1994).

3.3. Westerlies dominated western QB versus monsoon dominated CLP in the Quaternary

The western QB is out of the northern and western reach of the modern Asian summer monsoon (Gao, 1962) (Fig. 1). Water vapor flux analysis in the region of the Tibetan plateau also shows that the mid-latitude Westerlies dominate the atmospheric water vapor transport over and around the Tibetan plateau (Xu et al., 2008; Curio et al., 2015), and no substantial influence of the modern day EASM in the QB was detected in the High Asia Refined (HAR) reanalysis results (Curio et al., 2015). Therefore, we assume that water vapor supplied by the Westerlies and local water recycling are the main factors controlling the water balance in the QB region. In order to obtain insights into the driving mechanisms of the Qaidam paleolake evolution, and to explore what happened in other systems when the aforementioned critical phase transitions happened in the QB, we compare the trends in the evolution of the QB with records from the nearby CLP (Fig. 1), which is known to be controlled by the EASM. Similar trends and periodic behavior of the paleoclimate records from both regions may indicate a common forcing. In particular, a divergent pattern of evolution could indicate a varying regional expression of climatic patterns due to external forcing.

In Figs. 3 and 7 we compare the four proxy records from core SG-1 used in this study with climate records from the CLP reflecting the intensity of the EASM: the stacked summer monsoon index (SMI) from the Lingtai loess record (Sun et al., 2010) (Figs. 3G and 7B) and the χ record from the Chaona loess section (Song et al., 2001) (Fig. 3H). The drying trend detected in the QB from ~2.7 to ~1.2 Ma is synchronous with a weakening trend in the EASM (Fig. 7A and B). In contrast, the drying trend in the QB indicated by the records from

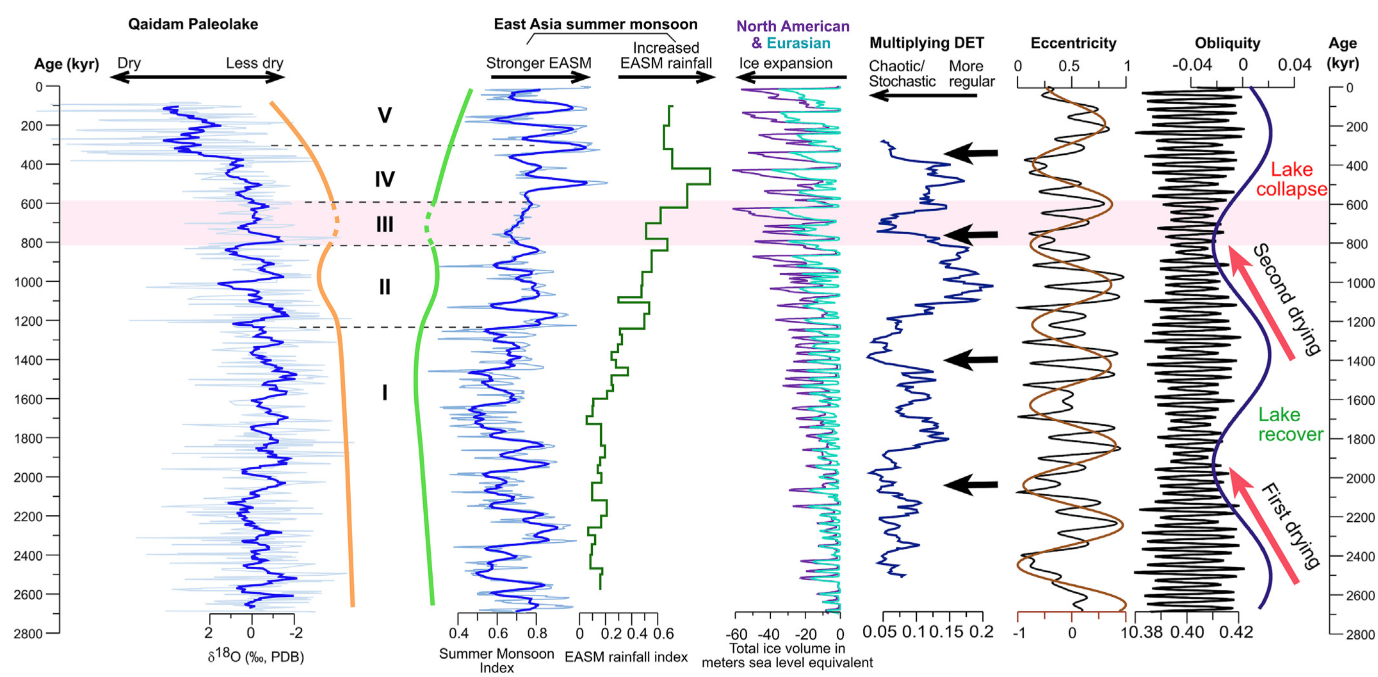

Fig. 7. Simple model displaying the evolution of the Qaidam paleolake and the EASM system. The five stages in paleolake evolution described in the text are shown in different color shades. (A) Qaidam paleolake evolution pattern represented by the $\delta^{18}O$ record from core SG-1. (B) EASM intensity variation represented by the summer monsoon index (SMI) of Sun et al. (2010), in which a higher SMI represents a stronger Asia summer monsoon. Thick lines in A and B are 41-kyr sliding window means of the records. (C) EASM rainfall index (Meng et al., 2018). (D) Modelled total ice volume for the North American and Eurasian ice sheets in meters sea level equivalent (deBoer et al., 2014). (E) Integrated determinism (DET) of the Qaidam paleolake (multiplying the DET results of SG-1 χ, Mz, Mn_{HOAc} and $\delta^{18}O$ records); black arrows represent abrupt decreases in the DET. (F) Eccentricity variation, with filtered 400-kyr variation highlighted. (G) Obliquity variation and filtered 1.2-Myr variation highlighted, with major drying trends of the Qaidam paleolake indicated by red arrows. (For interpretation of the references to color in this figure legend, the reader is referred to the Web version of this article.)

core SG-1 since ~1.2 Ma is accompanied by the trend of a slightly stronger EASM, as revealed by an increased SMI and higher magnetic susceptibility values in the Chinese Loess Plateau records (Fig. 3G and H, 7B). Therefore, it appears that both the QB and the CLP were primarily under the same climatic control before ~1.2 Ma, and changes in the driving mechanisms of the two systems (or different responses to a common forcing) led to a divergent pattern of the climatic evolution pattern between the two regions after ~1.2 Ma (Fig. 7A and B). The critical transition we identified in the QB from 0.8 to ~0.6 Ma is also prominent in the EASM record, in which an extremely less fluctuating EASM during ~0.9–0.8 to 0.6 Ma with slightly weaker intensity than before (Sun et al., 2010; Song et al., 2001), was succeeded by a strengthened EASM with large amplitude fluctuations (Fig. 3E and F). Song et al. (2001) and Sun et al. (2006) observed similar changes in the EASM at 0.62 Ma and 0.52 Ma, respectively. Paleosols in the CLP younger than 0.7 Ma are more developed, with clay-leached features and darker red color (Guo et al., 2000). An et al. (2005) interpreted carbon isotope records from the CLP by the replacement of a relatively stable EASM during 0.9–0.6 Ma that by a stronger EASM with the large expansion of C4 vegetation. Therefore, following a starting divergence in the QB and EASM systems at ~1.2 Ma and crossing of a critical transition at 0.8–0.6 Ma, a clear divergence of the two systems commenced after 0.6 Ma, when largely fluctuating conditions in the QB with a distinct drying trend were synchronous with strong fluctuations of the EASM and a trend of increasing humidity (Fig. 7A – C).

3.4. Possible driving mechanisms of the Qaidam paleolake evolution and critical transition at 0.8–0.6 Ma

A comparison of the determinism results of the SG-1 records with Earth orbital eccentricity (Supplementary Fig. S3A-F and Fig. 7E–G) reveals a similarity between the variation of determinism records and the 400-kyr component of eccentricity, with higher/lower values of eccentricity roughly corresponding to higher/lower values of the determinism, except for four specific intervals of ~2.4 to ~2.2 Ma, ~1.45 to ~1.2 Ma, ~0.8 to ~0.6 Ma and after ~0.4 Ma. Despite some differences for each proxy, there is a prominent decrease in the determinism of the records (Supplementary Fig. S3C-F and Fig. 7E) at these four intervals, indicating a change in system behavior from overall periodic to more irregular behavior (Marwan et al., 2007) at these intervals. This similarity between variations of the determinism records and the 400-kyr eccentricity implies a fundamental response of the lake system in the western QB to solar forcing. To further evaluate this, we performed a cross-correlation analysis between determinism of Mz and χ records and the 400-kyr eccentricity record (Supplementary Fig. S4E, F). During ~2.1 to ~1.5 Ma there is an overall high positive correlation, which indicates a relatively stable Qaidam lake system which responded about linearly to changes in solar insolation. The abrupt decrease in correlation and the shift to a high negative correlation during ~1.5 to ~1.3 Ma, and a pronounced negative correlation during ~2.4 to 2.2 Ma, ~1.5 to ~1.2 Ma and ~0.8–0.7 Ma indicate that the dynamical behavior of the lake system became less dependent on insolation forcing, or that there was a change in its response to insolation forcing at these intervals.

The meridional temperature gradient and poleward moisture transport controlled by obliquity are considered important factors for ice sheet growth in the Northern Hemisphere (Raymo and Nisancioglu, 2003; Loutre et al., 2004; Huybers and Wunsch, 2005). Reduced summer insolation at high latitudes during minima in the obliquity amplitude and in eccentricity would favour the reduction of snow and ice melting (Holbourn et al., 2018). It was suggested that the co-occurrence of minima in the obliquity amplitude and in eccentricity can facilitate the enhancement of glaciation via a sustained interval of reduced seasonal variability (Zachos et al., 2001; Pälike et al., 2006). In our proxy records from core SG-1, the first indication of drying in the QB starts at ~2.4 Ma, with its strongest representation at 2.2–2.1 Ma, which is supported by the first occurrence of salt layers (Wang et al., 2012) (Fig. 3A). This coincides with a decreasing amplitude of obliquity, beginning at ~2.4 Ma and reaching a minimum at ~1.9 Ma (Fig. 7F and G). This decrease may have facilitated the expansion of northern hemisphere ice sheets and intensified the drying in the QB, via its effects on moisture availability (Herb et al., 2015a), which would have resulted from the strengthening of the Siberian High and an increase in the intensity of the cold and dry winter monsoon (Guo et al., 2004; Yang et al., 2017). Ice expansion around 2.15–2.05 Ma as modelled total ice volume for the North American and Eurasian ice sheets (deBoer et al., 2014) (Fig. 7D) might serve as supporting evidence for this speculation. The first drop of determinism of SG-1 records (Supplementary Fig. S3C-F and Fig. 7E), which indicates a change of Qaidam lake system from a relatively stable (highly predictable) state to an unstable (less predictable) one during ~2.4 to 2.2 Ma, corroborates the interpretation that ice sheet expansion possibly disturbed the previous linear response of Qaidam lake system to the solar insolation change. However, the minimum in obliquity amplitude at ~1.9 Ma does not correspond to a minimum in eccentricity (Fig. 7F and G), indicating that limited effects on further amplification of ice sheet development, which eventually resulted in the disappearance of the salt layers and the recovery of the Qaidam lake system to a brackish lake (Wang et al., 2012) after ~2.1 Ma (Fig. 3A and B), with return to linear response to solar insolation change.

The next irregularity appears at another beginning of climate divergence at ~1.2 Ma, after the contemporaneous drying trend in both the QB and the CLP. After ~1.2 Ma, the two regions followed different trends of climatic evolution, with the strengthening of aridity in the QB (Fig. 7A) and a slight strengthening of the EASM in the CLP (Fig. 7B and C). This divergence corresponds to synchronous decreases in the determinism of the proxy records from core SG-1 and the EASM (Fig. 4D–F), with significant changes in correlation behavior between the determinism and eccentricity (Supplementary Fig. S4E, F). It represents a fundamental transition in the evolution of the two systems. The decreasing amplitude of obliquity that began at ~1.4 Ma, again corresponds to an eccentricity minimum at ~1.2 Ma, which would have promoted a sustained cold phase at high latitudes, an increase in the Northern Hemisphere ice sheets, and a strengthening of the Siberian High. Furthermore, decreased obliquity can facilitate strengthening of the Walker circulation (Philander and Fedorov, 2003). The persistent intensification of the Walker circulation during the period ~1.17–0.9 Ma (Liu and Herbert, 2004; de Garidel-Thoron et al., 2005; Medina-Elizalde and Lea, 2005; Lawrence et al., 2006) could also contribute to an increased water vapor supply from the subtropical northern Pacific area to the high latitudes of the Northern Hemisphere (McClymont and Rosell-Melé, 2005). The resulting ice sheet expansion and change in water vapor transport may have driven the system evolution in the QB and the CLP across a threshold at ~1.2 Ma, with internal forcing due to glaciation cycles and/or oceanic circulation changes playing an important role for both the Qaidam lake system and the EASM system. The effects of these factors appear to have replaced the previous dominant response of both system to solar insolation.

The subsequent co-occurrence of minima in the obliquity amplitude and in eccentricity from ~0.9 to 0.8 Ma (Fig. 7F and G) likely favored ice expansion (Zachos et al., 2001; Pälike et al., 2006; van Dam et al., 2006). In addition, the pronounced decrease in the atmospheric CO_2 level (Hönisch et al., 2009) that started at around

0.9 Ma is another important promoter for ice sheet growth (Clark et al., 2006; DeConto et al., 2008). These two factors might have pushed the growing ice sheets in northern hemisphere to a threshold state for climate impact in the Asia inland after 0.9–0.8 Ma. This is supported by the marine δ^{18}O record (Raymo, 1997; Lisiecki and Raymo, 2005; Elderfield et al., 2012), northern hemisphere ice-sheet reconstruction (Batchelor et al., 2019) and modelled ice volume (deBoer et al., 2014) records, which consistently indicate a striking expansion of northern hemisphere ice sheets at ~0.9–0.6 Ma, especially the Eurasian and North American ice sheets (deBoer et al., 2014; Batchelor et al., 2019) (Fig. 7D). The critical transition identified in the QB and the CLP systems at 0.8–0.6 Ma and the distinct divergence of two systems thereafter, characterized by largely fluctuating conditions in both systems accompanied by a distinct drying trend in QB and an increasing trend in the EASM (Fig. 7A – C), is contemporaneous with this striking ice expansion of northern hemisphere ice sheets, and may thus imply some relationship between them.

Modelling studies during the Last Glacial Maximum period corroborate an important role of increased northern hemisphere ice sheets on strengthening the meridional temperature gradient, and southward movement of the northern hemisphere Westerlies (COHMAP Members, 1988; Kutzbach et al., 1993; Wang et al., 2018). The expansion of northern hemisphere ice sheets and resulting global and regional cooling would contribute to a decrease of atmospheric moisture supply by the Westerlies to the QB due to decreased total water vapor in the atmosphere and a southward shift of the low level jet stream (Zhang and Delworth, 2005; Wang et al., 2018). Moreover, the transition of dominating cycles from ~41-kyr to ~100-kyr at ~1.2 Ma extended the time in which water was detracted from the Qaidam paleolake during cold glacial periods from previous 41-kyr to 100-kyr after ~1.2 Ma (Herb et al., 2015a). This would lead to a (too) long-term negative water balance of the regional water cycle of the QB catchment, and even a positive water cycle in interglacial periods may not be sufficient to return a lake that disappeared before as first the groundwater is filled. Such regional water cycle balancing has been recently corroborated by water balance analysis of the QB region (Scherer, 2020). As a possible consequence of ice expansion and prolongation of glacial periods, the water balance of the regional water cycle in the region of the QB that preserved the Qaidam paleolake became increasingly negative since 1.2 Ma.

The subsequent ice sheet growth at around 0.9–0.6 Ma, especially the significant expansion of Eurasian and North American ice sheets (deBoer et al., 2014; Batchelor et al., 2019) possibly exerted a profound influence on the Asian climate through facilitating an intense and zonally oriented northern hemisphere westerly jet (Oster et al., 2015; Löfverström et al., 2016) with a more southern position (Zhang and Delworth, 2005; Wang et al., 2018). In addition, modelling results indicated that the presence of Eurasia and North America ice sheets during MIS-13 would facilitate a strengthening of the EASM through an atmospheric wave train induced by ice sheet, or a positive phase of the winter North Atlantic Oscillation (NAO) like feature (Yin et al., 2008; Sundaram et al., 2012). This more equatorial and squeezed less wavy jet stream would place enlarged areas under the influence of cold airs, and thus facilitate colder/drier surface conditions in the Westerlies controlled QB area. It will possibly contribute to an increase of precipitation in the CLP area, either through a tilt of the summer rain band of the EASM which is located in the CLP area (Herzschuh et al., 2019) south of the Westerly jet (Sampe and Xie, 2010), or from an ice sheet expansion induced wave train which can facilitate EASM precipitation through strengthening of land-ocean thermal contrast resulting from enhanced warming over the Asian continent and cooling over the north-western Pacific (Sundaram et al., 2012). The described variation in the northern hemisphere ice sheets could explain the divergence between the Qaidam paleolake system and the EASM system that started from ~1.2 Ma and fully established after ~0.6 Ma. However, our hypothesis requires further reconnaissance on points such as ice-sheet variations during glacial and interglacial intervals and in particular the associated response in precipitation in the QB and CLP regions. Further modelling studies are needed to test and improve our hypothesis and to validate the existence of a critical shift in the regional water balance.

4. Conclusions

Comprehensive linear and nonlinear analyses of newly obtained and published data from the drill core SG-1 retrieved from the Westerlies dominated western Qaidam Basin (QB), and their comparison with records from the adjacent Chinese Loess Plateau (CLP) dominated by the East Asia Summer Monsoon (EASM) system, lead to the following results:

(1) The evolution of the QB lake system reached a critical transition at ~0.8–0.6 Ma, and the Qaidam paleolake collapsed without further recovery after ~0.6 Ma.
(2) We identify a similar evolution pattern of the lake system in the western QB and the CLP system from ~2.7 to ~1.2 Ma, and a divergence in the two systems that started at ~1.2 Ma and fully established after 0.6 Ma. After 0.6 Ma, largely fluctuating climate conditions and a distinct drying trend in the QB were accompanied by a synchronous strongly variable EASM with an increasing trend.
(3) We suggest that during 2.7–1.2 Ma, the QB and the CLP systems linearly responded to changes of solar insolation. This response was possibly disturbed by ice expansion in the northern hemisphere facilitated by the co-occurrence of low amplitudes in obliquity and a low eccentricity degree, leading to a divergent evolution of the two systems since 1.2 Ma. At ~0.9 to 0.8 Ma, a lowermost obliquity amplitude (node) and the synchronous minimum in eccentricity, together with a decrease in global atmospheric CO_2 concentration, could have jointly promoted the growth of northern hemisphere ice sheets cross a threshold in climate dynamics of the Asian inland. This striking ice expansion could have caused a more equatorial and zonally oriented northern hemisphere Westerly jet, placing the Westerlies controlled QB into the influence of colder and dryer airs, and contribute to the intensification of precipitation in the CLP area either through a tilt of the summer rain band of the EASM or an ice sheet expansion induced wave train. These effects explain the critical transition in the Qaidam paleolake evolution and the divergence between the QB and the CLP systems after ~0.6 Ma.

Author statement

We the undersigned declare that this manuscript is original, has not been published before and is not currently being considered for publication elsewhere.

We confirm that the manuscript has been read and approved by all named authors and that there are no other persons who satisfied the criteria for authorship but are not listed. We further confirm that the order of authors listed in the manuscript has been approved by all of us.

We understand that the Corresponding Author is the sole contact for the Editorial process. He/she is responsible for communicating with the other authors about progress, submissions of revisions and final approval of proofs.

Declaration of competing interest

We the undersigned declare that we have no known competing financial interests or personal relationships that could have appeared to influence the work reported in this paper.

Acknowledgements

This study was co-supported by the National Second Expedition to the Tibetan Plateau (2019QZKK0707), the Federal Ministry of Education and Research of Germany (BMBF) as part of the CAME II project (03G0863A), the Taishan Scholars Program of Shandong (tsqn201812102), and the National Science Foundation of China (grant 41571200). We gratefully acknowledge Yan Liu, Hui Yang, Wenyuan Han and Rongsheng Yang for their assistance in laboratory work, and Liang Yi and Chuanhe Lü for helpful discussions. Special thanks go to Deniz Eroglu and Bedartha Goswami for valuable suggestions on recurrence quantification analysis. We appreciate the Editor and two anonymous reviewers for their valuable comments and constructive suggestions. The data supporting the findings of the study are available in the PANGAEA data center https://doi.pangaea.de/10.1594/PANGAEA.904354.

Appendix A. Supplementary data

Supplementary data to this article can be found online at https://doi.org/10.1016/j.quascirev.2020.106580.

References

An, Z.S., Liu, T.S., Lu, Y.C., Porter, S.C., Kukla, G., Wu, X.H., Hua, Y.M., 1990. The long-term Paleomonsoon variation recorded by the loess–paleosol sequence in central China. Quat. Int. 7 (8), 91–95.
An, Z.S., Colman, S.M., Zhou, W., Li, X., Brown, E.T., Jull, A.J.T., et al., 2012. Interplay between the Westerlies and Asian monsoon recorded in lake Qinghai sediments since 32 ka. Sci. Rep. 2 (1), 619. https://doi.org/10.1038/srep00619.
An, Z., Huang, Y., Liu, W., Guo, Z., Clemens, S.C., Li, L., Prell, W.L., Cai, Y., Zhou, W., Lin, B., 2005. Multiple expansions of C4 plant biomass in East Asia since 7 Ma coupled with strengthened monsoon circulation. Geology 33, 705–708.
Batchelor, C.L., Margold, M., Krapp, M., et al., 2019. The configuration of Northern Hemisphere ice sheets through the Quaternary. Nat. Commun. 10 (1), 1–10.
Blott, S., Pye, K., 2001. GRADISTAT: a grain size distribution and statistics package for the analysis of unconsolidated sediments. Earth Surf. Process. Landforms 26 (11), 1237–1248.
Chen, F., Yu, Z., Yang, M., Emi, i., Wang, S., David, B., Huang, X., Zhao, Y., Tomonori, S., John, B.B., 2008. Holocene moisture evolution in arid central Asia and its out-of-phase relationship with Asian monsoon history. Quat. Sci. Rev. 27, 351–364.
Cai, M., Fang, X., Wu, F., Miao, Y., Appel, E., 2012. Pliocene–Pleistocene stepwise drying of Central Asia: evidence from paleomagnetism and sporopollen record of the deep borehole SG-3 in thewestern Qaidam Basin, NE Tibetan Plateau. Global Planet. Change 94-95, 72–81.
Chen, F., Chen, J., Huang, W., Chen, S., Huang, X., Kaser, G., Bolch, T., Marzeion, B., Gardelle, J., Zhang, G., 2019. Westerlies Asia and monsoonal Asia: spatiotemporal differences in climate change and possible mechanisms on decadal to sub-orbital timescales. Earth Sci. Rev. 192, 337–354.
Clark, P.U., Archer, D., Pollard, D., Blum, J.D., Rial, J.A., Brovkin, V., Mix, A.C., Peter, U., Nicklas, G., Alan, C., 2006. The Middle Pleistocene transition: characteristics, mechanisms, and implications for long-term changes in atmospheric pCO2. Quat. Sci. Rev. 25, 3150–3184.
Curio, J., Maussion, F., Scherer, D., 2015. A 12 year high resolution climatology of atmospheric water transport over the Tibetan plateau. Earth Syst. Dynam. 6 (1), 109124.
De Garidel-Thoron, T., Rosenthal, Y., Bassinot, F., Beaufort, L., 2005. Stable sea surface temperatures in the western Pacific warm pool over the past 1.75 million years. Nature 433, 294–298.
deBoer, B., Lourens, L.J., vandeWal, R.S.W., 2014. Persistent 400,000-year variability of Antarctic ice volume and the carbon cycle is revealed throughout the Plio-Pleistocene. Nat. Commun. 5, 2999.
DeConto, R.M., Pollard, D., Wilson, P.A., Pälike, H., Lear, C.H., Pagani, M., 2008. Thresholds for Cenozoic bipolar glaciation. Nature 455, 652–656.
Ding, Z.L., Liu, T.S., Rutter, R.W., Yu, Z.W., Guo, Z.T., Zhu, R.X., 1995. Ice-volume forcing of East Asian winter monsoon variations in the past 800,000 years. Quat. Res. 44, 149–159.
Ding, Z., Ranov, V., Yang, S., Finaev, A., Han, J., Wang, G., 2002. The loess record in southern Tajikistan and correlation with Chinese loess. Earth Planet Sci. Lett. 200, 387–400.
Ding, Z., Derbyshire, E., Yang, S., Sun, J., Liu, T., 2005. Stepwise expansion of desert environment across northern China in the past 3.5 Ma and implications for monsoon evolution. Earth Planet Sci. Lett. 237 (1–2), 45–55.
Donges, J.F., Donner, R.V., Trauth, M.H., Marwan, N., Schellnhuber, H.J., Kurths, J., 2011. Nonlinear detection of paleoclimate-variability transitions possibly related to human evolution. Proc. Natl. Acad. Sci. U. S. A 108, 20423–20428.
Eckmann, J., Oliffson Kamphorst, S., Ruelle, D., 1987. Recurrence plots of dynamical systems. Europhys. Lett. 4 (91), 973–977.
Elderfield, H., Ferretti, P., Greaves, M., Crowhurst, S., McCave, I.N., Hodell, D., Piotrowski, A.M., 2012. Evolution of ocean temperature and ice volume through the Mid-Pleistocene Climate Transition. Science 337, 704–707.
Eroglu, D., McRobie, F.H., Ozken, I., Stemler, T., Wyrwoll, K.H., Breitenbach, S.F.M., Mann, M.E., Yan, H., Wang, Y., Wu, R., 2016. See–saw relationship of the Holocene East Asian–Australian summer monsoon. Nat. Commun. 7, 12929.
Fang, X.M., Li, J.J., Vander Voo, R., 1999. Rock magnetic and grain size evidence for intensified Asian atmospheric circulation since 800,000 years B.P. related to Tibetan uplift. Earth Planet. Sci. Lett. 165, 129–144.
Fang, X., Shi, Z., Yang, S., Wu, F., Ma, Y., An, Z., Li, J., 2002. Loess in the tian Shan and its implications for the development of the Gurbantunggut Desert and drying of northern xinjiang. Chin. Sci. Bull. 47 (16), 1381–1387.
Ghil, M., 1994. Cryothermodynamics: the chaotic dynamics of paleoclimate. Phys. Nonlinear Phenom. 77 (1–3), 130–159.
Guo, Z., Biscaye, P., Wei, L., Chen, X., Peng, S., Liu, T., 2000. Summer monsoon variations over the last 1.2 Ma from the weathering of loess-soil sequences in China. Geophys. Res. Lett. 27, 1751–1754.
Guo, Z., Peng, S., Hao, Q., Biscaye, P.E., An, Z., Liu, T., 2004. Late miocene–pliocene development of asian aridification as recorded in the red-earth formation in northern China. Global Planet. Change 41, 135–145.
Han, W., Fang, X., Ye, C., Teng, X., Zhang, T., 2014a. Tibet forcing Quaternary stepwise enhancement of westerly jet and central Asian aridification: carbonate isotope records from deep drilling in the Qaidam salt playa, NE Tibet. Global Planet. Change 116, 68–75.
Han, W., Ma, Z., Lai, Z., Appel, E., Fang, X., Yu, L., 2014b. Wind erosion on the northeastern Tibetan Plateau: constraints from OSL and U-Th dating of playa salt crust in the Qaidam Basin. Earth Surf. Process. Landforms 39, 779–789.
Herb, C., Zhang, W., Koutsodendris, A., Appel, E., Fang, X., Pross, J., 2013. Environmental implications of the magnetic record in Pleistocene lacustrine sediments of the Qaidam Basin, NE Tibetan Plateau. Quarter. Int. 313–314, 218–229.
Herb, C., Koutsodendris, A., Zhang, W., Appel, E., Fang, X., Voigt, S., Pross, J., 2015a. Late Plio–Pleistocene humidity fluctuations in the western Qaidam Basin (NE Tibetan Plateau) revealed by an integrated magnetic-palynological record from lacustrine sediments. Quat. Res. 84, 457–466.
Herb, C., Appel, E., Voigt, S., Koutsodendris, A., Pross, J., Zhang, W., Fang, X., 2015b. Orbitally tuned age model for the Late Pliocene–Pleistocene lacustrine succession of drill core SG-1 from the western Qaidam Basin (NE Tibetan Plateau). Geophys. J. Int. 200, 35–51.
Herzschuh, U., Cao, X.Y., Laepple, T., Dallmeyer, A., Telford, R.J., et al., 2019. Position and orientation of the westerly jet determined Holocene rainfall patterns in China. Nat. Commun. 10, 2376.
Holbourn, A.E., Kuhnt, W., Clemens, S.C., Kochhann, K.G.D., Jöhnck, J., Lübbers, J., Andersen, N., 2018. Late Miocene climate cooling and intensification of Southeast Asian winter monsoon. Nat. Commun. 9, 1584.
Huybers, P., 2009. Pleistocene glacial variability as a chaotic response to obliquityforcing. Clim. Past 5 (3), 481–488.
Huybers, P., Wunsch, C., 2005. Obliquity pacing of the late Pleistocene glacial terminations. Nature 434, 491–494.
Hönisch, B., Hemming, N.G., Archer, D., Siddall, M., McManus, J., 2009. Atmospheric carbon dioxide concentration across the mid-Pleistocene transition. Science 324, 1551–1554.
Kang, A., Zhu, X., Han, D., Wang, Y., Kang, Q., 2003. Quaternary sporopollen assemblages and paleoclimatic fluctuation in the Qaidam Basin. Geol. Bull. China 22, 12–15.
Koutsodendris, A., Sachse, D., Appel, E., Herb, C., Fischer, T., Fang, X., Pross, J., 2018. Prolonged monsoonal moisture availability preconditioned glaciation of the Tibetan Plateau during the Mid-Pleistocene Transition. Geophys. Res. Lett. 45.
Kutzbach, J., Gutter, P., Behling, P.J., Selin, R., 1993. In: Global Climates since the Last Glacial Maximum. Wright H. E. Univ. of Minnesota Press, MN, pp. 24–93.
Lawrence, K.T., Liu, Z., Herbert, T.D., 2006. Evolution of the eastern tropical pacific through plio-pleistocene glaciation. Science 312, 79–83.
Lawrence, K.T., Herbert, T.D., Brown, C.M., Raymo, M.E., Haywood, A.M., 2009. High amplitude variations in North Atlantic sea surface temperature during the early Pliocene warm period. Paleoceanography 24, PA2218.
Lenton, T.M., 2011. Early warning of climate tipping points. Nat. Clim. Change 1, 201–209.
Li, G., Rao, Z., Duan, Y., Xia, D., Wang, L., Madsen, D.B., Jia, J., Qiang, M., Chen, J., Chen, F., 2016. Paleoenvironmental changes recorded in a luminescence dated loess/paleosol sequence from the Tianshan Mountains, arid Central Asia, since the Penultimate Glaciation. Earth Planet Sci. Lett. 448, 1–12.
Lisiecki, L., Raymo, M.A., 2005. Pliocene-Pleistocene stack of 57 globally distributed benthic $\delta^{18}O$ records. Paleoceanography 20, PA1003.
Liu, T.S., Ding, Z.L., 1993. Stepwise coupling of monsoon circulation to global ice volume variations during the late Cenozoic. Global Planet. Change 7, 119–130.

Liu, Z., Herbert, T.D., 2004. High-latitude influence on the eastern equatorial Pacific climate in the early Pleistocene epoch. Nature 427, 720–723.
Löfverström, M., Caballero, R., Nilsson, J., Messori, G., 2016. Stationary wave reflection as a mechanism for zonalizing the Atlantic winter jet at the LGM. J. Atmos. Sci. 73, 3329–3342. https://doi.org/10.1175/JAS-D-15-0295.1.
Loutre, M.F., Paillard, D., Vimeux, F., Cortijo, E., 2004. Does mean annual insolation have the potential to change the climate? Earth Planet Sci. Lett. 221, 1–14.
Lu, H., An, Z., 1997. Experimental study on the influence of different pretreatment procedures on the particle-size measurement of loess sediments. Chin. Sci. Bull. 42, 2535–2538.
Lu, H., Wang, X., Li, L., 2010. Aeolian sediment evidence that global cooling has driven late Cenozoic stepwise aridification in Central Asia. Geol. Soc. Lond., Spec. Publ. 342 (1), 29–44. https://doi.org/10.1144/SP342.4.
Maasch, K., Saltzman, B., 1990. A low-order dynamic model of global climate variability over the full Pleistocene. J. Geophys. Res. 95 (D2), 1955–1963.
Marwan, N., Romano, M.C., Thiel, M., Kurths, J., 2007. Recurrence plots for the analysis of complex systems. Phys. Rep. 438, 237–329.
Marwan, N., Eroglu, D., Ozken, I., Stemler, T., Wyrwoll, K.H., Kurths, J., 2017. Regime change detection in irregularly sampled time series. In: Advances in Nonlinear Geosciences. Springer, pp. 357–368.
McClymont, E.L., Rosell-Melé, A., 2005. Links between the onset of modern Walker circulation and the mid-Pleistocene climate transition. Geology 33, 389–392.
McKenzie, J.A., 1985. Carbon isotopes and productivity in the lacustrine and marine environment. In: Stumm, W. (Ed.), Chemical Processes in Lakes. Wiley, New York, pp. 99–118.
Medina-Elizalde, M., Lea, D.W., 2005. The Mid-Pleistocene transition in the tropical Pacific. Science 310, 1009–1012.
COHMAP Members, 1988. Climatic changes of the last 18,000 years: observations and model simulations. Science 241, 1043–1052.
Meng, X.Q., Liu, L.W., Wang, X., Balsam, W., Chen, J., Ji, J.F., 2018. Mineralogical evidence of reduced East Asian summer monsoon rainfall on the Chinese loess plateau during the early Pleistocene interglacials. Earth Planet Sci. Lett. 486, 61–69.
Mudelsee, M., Stattegger, K., 1997. Exploring the structure of the mid-Pleistocene revolution with advance methods of time-series analysis. Geol. Rundsch. 86, 499–511.
Oster, J.L., Ibarra, D.E., Winnick, M.J., Maher, K., 2015. Steering of westerly storms over western north America at the last glacial Maximum. Nat. Geosci. 8, 201–205.
Pälike, H., Jens, O., Paul, A., Henel, K., Richard, D., Bridget, S., 2006. The heartbeat of the oligocene climate system. Science 314, 1894–1898.
Philander, S., Fedorov, A.V., 2003. Role of tropics in changing the response to Milankovich forcing some three million years ago. Paleoceanography 18, 1045.
Raymo, M., 1997. The timing of major climate terminations. Paleoceanography 12, 577–585.
Raymo, M., Nisancioglu, K., 2003. The 41 kyr world: milankovitch's other unsolved mystery. Paleoceanography 18, 1011.
Sampe, T., Xie, S., 2010. Large-scale dynamics of the Meiyu-Baiu rainband: environmental forcing by the Westerly Jet. J. Clim. 23, 113–134.
Scheffer, M., Bacompte, J., Brock, W.A., Brovkin, V., Carpenter, S.R., Dakos, V., 2009. Early warning signals for critical transitions. Nature 461, 53–59.
Scherer, D., 2020. Survival of the Qaidam mega-lake system under mid-Pliocene climates and its restoration under future climates. Hydrol. Earth Syst. Sci. 24, 3835–3850.
Schmieder, F., Von Dobeneck, T., Bleil, U., 2000. The Mid-Pleistocene climate transition as documented in the deep South Atlantic Ocean: initiation, interim state and terminal event. Earth Planet Sci. Lett. 179, 539–549.
Shackleton, N.J., Berger, A., Peltier, W.R., 1990. An alternative astronomical calibration of the Lower Pleistocene timescale based on ODP Site 677. In: Transactions of the Royal Society of Edinburgh, vol. 81. Earth Science (Earth Env. Sci. T. R. So.), pp. 251–261.
Song, Y., Fang, X., Masayuki, T., Naoto, I., Li, J., An, Z., 2001. Magnetostratigraphy of late tertiary sediments from the Chinese Loess Plateau and its paleoclimatic significance. Chin. Sci. Bull. 46, 16–21.
Sun, Y., Clemens, S.C., An, Z., Yu, Z., 2006. Astronomical timescale and palaeoclimatic implication of stacked 3.6-Myr monsoon records from the Chinese Loess Plateau. Quat. Sci. Rev. 25 (1–2), 33–48.
Stuiver, M., 1970. Oxygen and carbon isotope ratios of fresh-water carbonates as climatic indicators. J. Geophys. Res. 75, 5247–5257.
Sun, Y., An, Z., Clemens, S.C., Bloemendal, J., Vandenberghe, J., 2010. Seven million years of wind and precipitation variability on the Chinese Loess Plateau. Earth Planet Sci. Lett. 297 (3–4), 525–535.
Sundaram, S., Yin, Q.Z., Berger, A., Muri, H., 2012. Impact of ice sheet induced North Atlantic oscillation on East Asian summer monsoon during an interglacial 500,000 years ago. Clim. Dynam. 39, 1093–1105.
Talbot, M.R., 1990. A review of the palaeohydrological interpretation of carbon and oxygen isotopic ratios in primary lacustrine carbonates. Chem. Geol. 80, 261–279.
Talbot, M.R., Kelts, K., 1990. Paleolimnological signatures fromcarbon and oxygen isotopic ratios in carbonates from organic carbon-rich lacustrine sediments. AAPG Mem 50, 61–76.
Torrence, D.C., Compo, G.P., 1998. A practical guide to wavelet analysis. Bull. Am. Meteorol. Soc. 79, 61–78.
van Dam, J.A., Abdul Aziz, H., Álvarez Sierra, M.A., Hilgen, F.J., van den Hoek Ostende, L.W., Lourens, L.J., Mein, P., van der Meulen, A.J., Peláez-Campomanes, P., 2006. Long-period astronomical forcing of mammal turnover. Nature 433, 687–691.
Vandenberghe, J., 2013. Grain size of fine-grained windblown sediment: a powerful proxy for process identification. Earth Sci. Rev. 121, 18–30. https://doi.org/10.1016/j.earscirev.2013.03.001.
Vandenberghe, J., Sun, Y.B., Wang, X.Y., Abels, H.A., Liu, X.X., 2018. Grain-size characterization of reworked fine-grained aeolian deposits. Earth Sci. Rev. 177, 43–52.
Wang, J., 2012. Sedimentary Evolution of Chahansilatu Depression in Western Qaidam Basin since 2.8Ma and Aridification of Asian Interior. PhD Thesis. University of Chinese Academy of Sciences, p. 154.
Wang, J., Fang, X., Appel, E., Song, C., 2012. Pliocene-Pleistocene climate change at the N E Tibetan Plateau deduced from lithofacies variation in the drilling core SG-1, western Qaidam Basin. J. Sediment. Res. 82, 933–952.
Wang, P., Wang, B., Cheng, H., Fasullo, J., Guo, Z., Kiefer, T., Liu, Z., 2017. The global monsoon across time scales: mechanisms and outstanding issues. Earth Sci. Rev. 174, 84–121.
Wang, N., Jiang, D., Lang, X., 2018. Northern westerlies during the last glacial Maximum: results from CMIP5 simulations. J. Clim. 31, 1135–1153.
Wissel, C., 1984. A universal law of the characteristic return time near thresholds. Oecologia 65, 101–107.
Xiao, J.L., An, Z.S., 1999. Three large shifts in East Asian monsoon circulation indicated by loess–paleosol sequences in China and Late Cenozoic deposits in Japan. Palaeogeogr. Palaeoclimatol. Palaeoecol. 154 (3), 179–189.
Xu, X., Lu, C., Shi, X., Gao, S., 2008. World water tower: an atmospheric perspective. Geophys. Res. Lett. 35, L20815.
Yang, S., Ding, F., Ding, Z., 2006. Pleistocene chemical weathering history of Asian arid and semi-arid regions recorded in loess deposits of China and Tajikistan. Geochem. Cosmochim. Acta 70, 1695–1709.
Yang, Y., Fang, X., Appel, E., Galy, A., Li, M., Zhang, W., 2013a. Late Pliocene–Quaternary evolution of redox conditions in the western Qaidam paleolake (NE Tibetan Plateau) deduced from Mn geochemistry in the drilling core SG-1. Quat. Res. 80, 586–595.
Yang, Y., Fang, X., Galy, A., Appel, E., Li, M., 2013b. Quaternary paleolake nutrient evolution and climatic change in the western Qaidam Basin deduced from phosphorus geochemistry record of deep drilling core SG-1. Quat. Int. 313–314, 156–167.
Yang, Y., Fang, X., Galy, A., Li, M., Appel, E., Liu, X., 2014. Paleoclimatic significance of rare earth element record of the calcareous lacustrine sediments from a long core (SG-1) in the western Qaidam Basin, N E Tibetan Plateau. J. Geochem. Explor. 145, 223–232.
Yang, Y., Fang, X., Koutsodendris, A., Ye, C., Yang, R., Zhang, W., Liu, Xiaoming, Gao, S., 2016. Exploring Quaternary paleolake evolution and climate change in the western Qaidam basin based on the bulk carbonate geochemistry of lake sediments. Palaeogeogr. Palaeoclimatol. Palaeoecol. 446, 152–161.
Yang, Y., Yang, R., Li, X., Han, W., Zan, J., 2017. Glacial-interglacial climate change on the northeastern Tibetan Plateau over the last 600 kyr. Palaeogeogr. Palaeoclimatol. Palaeoecol. 476, 181–191.
Yin, Q.Z., Berger, A., Driesschaert, E., Goosse, H., Loutre, M.F., Crucifix, M., 2008. The Eurasian ice sheet reinforces the East Asian summer monsoon during the interglacial 500,000 years ago. Clim. Past 4, 79–90.
Zachos, J.C., Shackleton, N.J., Revenaugh, J.S., Pälike, H., Flower, B.P., 2001. Climate response to orbital forcing across the oligocene-miocene boundary. Science 292, 274–278.
Zan, J., Fang, X., Yang, S., 2010. A rock magnetic study of loess from the West Kunlun Mountains. J. Geophys. Res. 115 (B10), B10101.
Zhang, R., Delworth, T.L., 2005. Simulated tropical response to a substantial weakening of the Atlantic thermohaline circulation. J. Clim. 18, 1853–1860.
Zhang, W., Appel, E., Fang, X., Song, C., Hu, S., Liu, D., Cirpka, O., 2012a. Magnetostratigraphy of deep drilling core SG-1 in the western Qaidam Basin (NE Tibetan Plateau) and its tectonic implications. Quat. Res. 78, 139–148.
Zhang, W., Appel, E., Fang, X., Yan, M., Song, C., Cao, L., 2012b. Paleoclimatic implications of magnetic susceptibility in Late Pliocene–Quaternary sediments from deep drilling core SG-1 in the western Qaidam Basin (NE Tibetan Plateau). J. Geophys. Res. 117, B06101.